communications chemistry

A Nature Portfolio journal

Article

https://doi.org/10.1038/s42004-025-01466-6

Ca^{2+}-triggered allosteric catalysts crosstalk with cellular redox systems through their foldase- and reductase-like activities

Rumi Mikami[1], Yuhei Sato[1], Shingo Kanemura[2], Takahiro Muraoka[3,4], Masaki Okumura[2,5] & Kenta Arai[1,6]

Effective chemical catalysts can artificially control intracellular metabolism. However, in conventional catalytic chemistry, activity and cytotoxicity have a trade-off relationship; thus, driving catalysts in living cells remains challenging. To overcome this critical issue at the interface between catalytic chemistry and biology, we developed cell-driven allosteric catalysts that exert catalytic activity at specific times. The synthesized allosteric redox catalysts up- and downregulated their foldase- and antioxidase-like activities in response to varying Ca^{2+} concentrations, which is a key factor for maintenance of the redox status in cells. In the absence of Ca^{2+} or at low Ca^{2+} concentrations, the compounds were mostly inactive and hence did not affect cell viability. In contrast, under specific conditions with elevated cytosolic Ca^{2+} concentrations, the activated compounds resisted the redox imbalance induced by the reactive oxygen species generated by Ca^{2+}-stimulated mitochondria. Smart catalysts that crosstalk with biological phenomena may provide a platform for new prodrug development guidelines.

Metabolic disorders in living cells lead to undesired chemical phenomena such as oxidative stress[1–3], protein misfolding[4,5], glycative stress[6,7], and nucleic acid modification[8–10], eventually causing irreversible cellular pathological degeneration. Chemical small molecules would be useful for artificially regulating cellular homeostasis by aiding and enhancing the functions of enzymes, which are responsible for the order of intracellular chemical reactions. This approach can expand the range of therapeutic strategies for various diseases. Although small organocatalysts with enzyme-like functions, such as small catalysts with high reactivity, have been developed in recent decades, they often cause nonspecific reactions in cells, leading to catalyst inactivation and cytotoxicity[11]. Therefore, novel biocompatible molecules that incorporate the spatiotemporal concept are needed to exert appropriate physiological activity at appropriate times in specific cellular compartments.

Allosteric enzymes, which are responsible for the space-time dynamics of intracellular reaction fields, are representative biomolecular machinery that modulate the intensity of catalytic activities and substrate selectivity in response to their own structural changes triggered by allosteric effectors (Fig. 1a, left)[12]. Controlling a reaction system consisting of multiple elementary reactions is typically difficult, even in a flask where the solvent, additive, and temperature can be changed arbitrarily. Nonetheless, several catalysts that mimic the functions of allosteric enzymes have been developed in recent years, enabling better control of complex reaction systems in flasks[13–16]. These catalysts can modulate their catalytic activities by changing their molecular structure in response to external stimuli (e.g., light, temperature, pH, and ion strength) and promote or inhibit a specific reaction. However, the application of artificial catalysts has been largely limited to reactions in organic solvents[17]. Although numerous studies have focused on overcoming this issue[18–20], in-cell-driven allosteric catalysts that crosstalk with biological phenomena in living cells have not been explored.

[1]Department of Chemistry, School of Science, Tokai University, 4-1-1 Kitakaname, Hiratsuka-shi, Kanagawa, Japan. [2]Frontier Research Institute for Interdisciplinary Sciences, Tohoku University, 6-3 Aramakiaza Aoba, Aoba-ku, Sendai, Miyagi, Japan. [3]Department of Applied Chemistry, Graduate School of Engineering, Tokyo University of Agriculture and Technology, 2-24-16 Naka-cho, Koganei, Tokyo, Japan. [4]Kanagawa Institute of Industrial Science and Technology, 3-2-1 Sakato, Takatsu-ku, Kawasaki, Kanagawa, Japan. [5]Department of Molecular and Chemical Life Sciences, Graduate School of Life Sciences, Tohoku University, 2-1-1 Katahira, Aoba-Ku, Sendai, Miyagi, Japan. [6]Institute of Advanced Biosciences, Tokai University, 4-1-1 Kitakaname, Hiratsuka-shi, Kanagawa, Japan. e-mail: k-arai4470@tokai-u.jp; ak5638@tokai.ac.jp

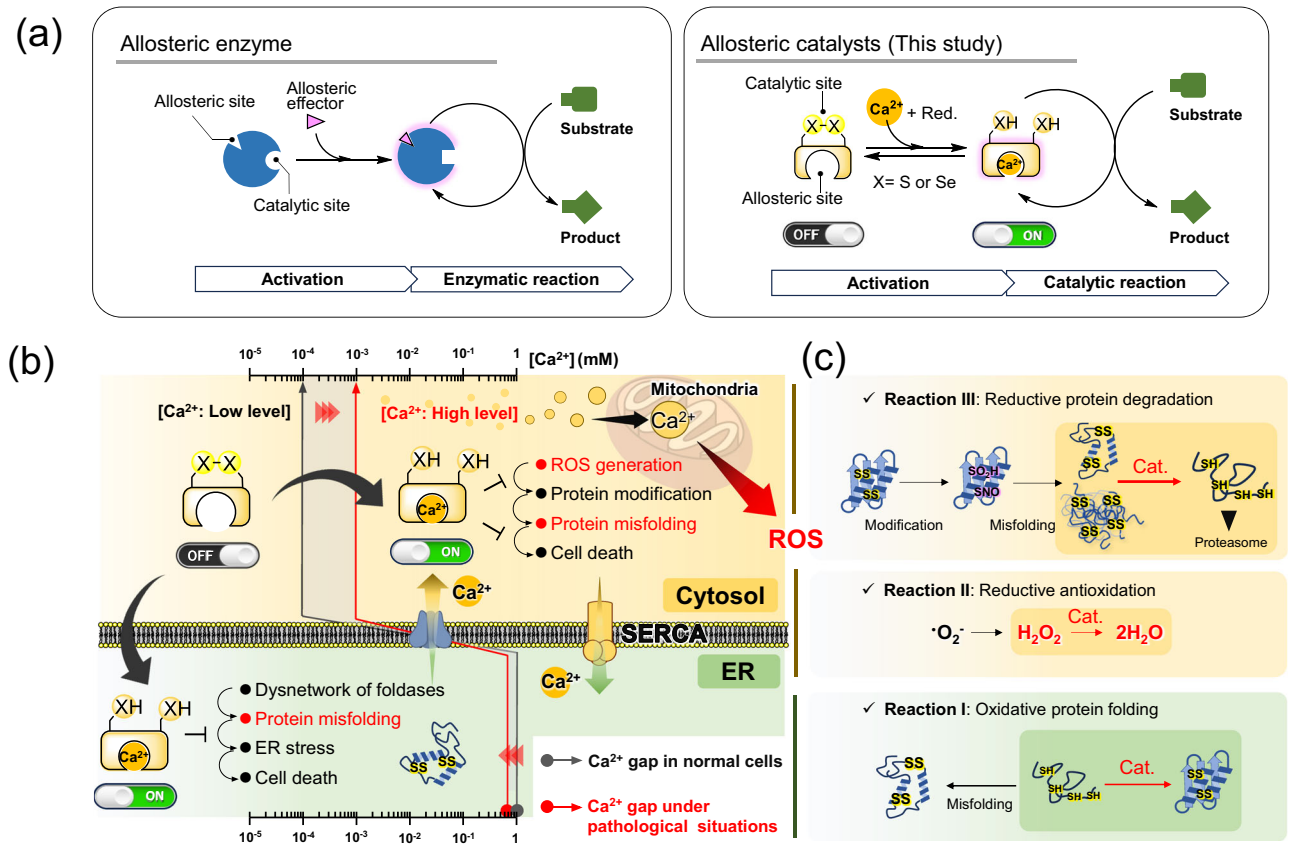

Fig. 1 | Biological redox reactions in response to changes in Ca^{2+} concentration. **a** Action of enzyme (left) and an artificial enzyme-like catalyst (right) regulated by an allosteric effector. **b** Crosstalk between Ca^{2+}-triggered allosteric S–S- or Se–Se-catalyst and redox imbalance induced by abnormal fluctuation of the Ca^{2+} concentration. **c** Model bio-related redox reactions (I–III) up- and downregulated by Ca^{2+}-triggered catalysts.

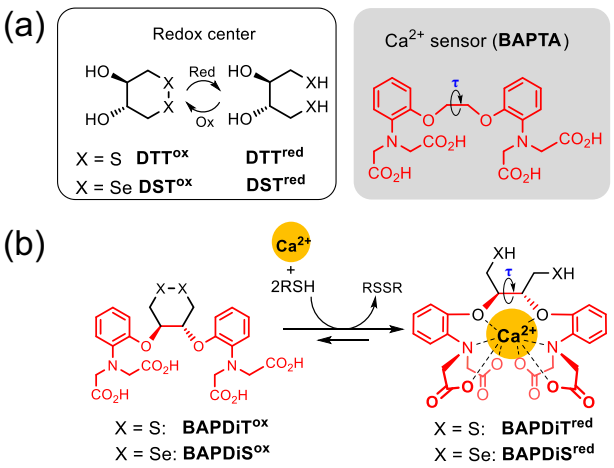

Fig. 2 | Molecular design of Ca^{2+}-sensing-redox compounds. **a** Molecular structure of $DTT^{ox/red}$, $DST^{ox/red}$ and BAPTA as a Ca^{2+}-selective chelator. **b** BAPTA-fused DTT^{ox} and DST^{ox}, namely $BAPDiT^{ox}$ and $BAPDiS^{ox}$, respectively, which can be activated to the corresponding chalcogenol states in the presence of Ca^{2+}.

Redox reactions are essential for maintaining cellular homeostasis. An imbalance in the redox system in cells leads to the production of pathogenic substances such as reactive oxygen species (ROS) and misfolded proteins[21,22]. Thiolate (S^-) and selenolate (Se^-) anions, which are the deprotonated states of cysteinyl thiol (SH) and selenocysteinyl selenol (SeH), respectively, act as excellent two-electron donors at the active centers of various oxidoreductases. We previously developed small SH- and SeH-based catalysts that mimic the activities of oxidoreductases involved in oxidative folding[23–27] and reductive antioxidation[28,29]. Protein disulfide isomerase (PDI) is an endoplasmic reticulum (ER)-resident oxidoreductase that catalyzes folding coupled with disulfide (S–S) bond formation between Cys residues (oxidative folding) in nascent polypeptides[30–36]. Two CGHC tetrapeptides, which constitute the catalytic sites in PDI, catalytically isomerize mis-bridged S–S bonds in substrate proteins to the correct S–S-bonding pattern found in the native state through their high nucleophilic capability of cysteinyl SH groups (for more information on the catalytic mechanisms of PDI, see Results). In the presence of a reducing agent, *trans*-4,5-dihydroxy-1,2-dithiane (DTT^{ox})[37] and its diselenide (Se–Se) analog (DST^{ox})[23] are reversibly activated into the ring-opened states, DTT^{red} and DST^{red}, respectively (Fig. 2a, left). These structures promote S–S isomerization during oxidative folding through a molecular mechanism similar to that of PDI. Glutathione peroxidase (GPx) is a representative selenoenzyme with a selenocysteine residue in the active center, which catalytically reduces hydroperoxides with glutathione (GSH) as a co-substrate[38,39]. DST^{red} shows much higher GPx-like activity than does DTT^{red} because the SeH group has a higher electron-donating capacity than that of the SH group[29,40]. Organochalcogenic compounds are promising surrogates for oxidoreductases that maintain cellular redox homeostasis[41]. However, such reagents, which are highly reactive but nonspecific, are often cytotoxic. Consequently, they have been applied to in-cell and in vivo experiments in only a few cases[42,43].

To ensure that our established minimal oxidereductase-like catalysts can appropriately exhibit high activity in specific situations, we fused them with an activity-switching sensor (Fig. 1a, right). Several metal ions are abundant and ubiquitous in cells, and their concentrations vary widely and reversibly in signaling pathways. Hence, the quantitative properties of metal ions may be useful as triggers to turn the activity of the artificial catalyst in

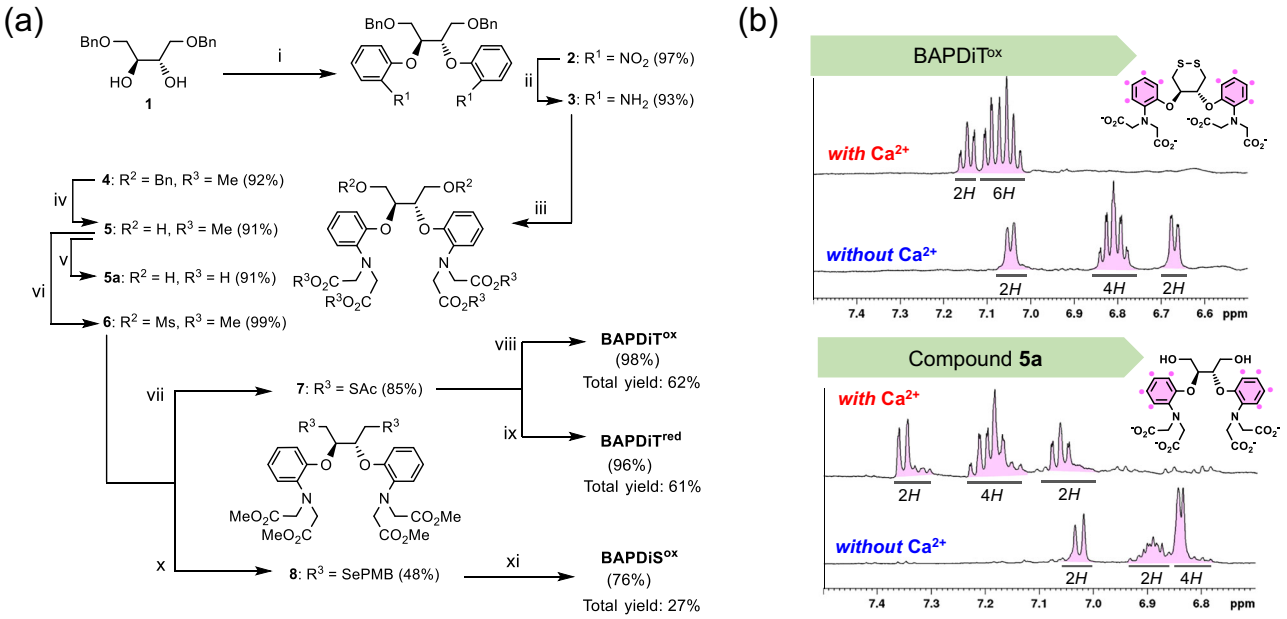

Fig. 3 | Synthesis of Ca^{2+}-sensing-redox compounds. a Synthetic routes for $BAPDiT^{ox}$, $BAPDiT^{red}$, and $BAPDiS^{ox}$. Starting material **1** was prepared in 51% overall yield through 3 steps as described previously (see Supplementary Information). Reaction conditions: (i) NaH and 2-fluoronitrobenzene in dimethylformamide (DMF) at 120 °C for 19 h; (ii) Zn and acetic acid (AcOH) in tetrahydrofuran (THF)/methanol (MeOH) at 25 °C for 17 h; (iii) NaI, proton sponge, and methyl bromoacetate in CH_3CN for 16 h under the reflux condition; (iv) H_2 and Pd/C in MeOH at 25 °C for 22 h; (v) KOH in THF/MeOH at 25 °C for 2 h; (vi) MsCl in pyridine at 0 °C for 2 h; (vii) KSAc in DMF at 60 °C for 2 h; (viii) KOH in THF/MeOH at 25 °C for 3 h, and then H_2O_2 at 25 °C for 0.5 h; (ix) KOH in THF/MeOH at 25 °C for 3 h, and then TCEP at 25 °C for 1 h; (x) $(PMBSe)_2$ and $NaBH_4$ in THF/EtOH for 2.5 h under the reflux condition; (xi) I_2 in $MeOH/H_2O$ at 25 °C for 2 h, and then KOH in THF/MeOH. **b** ^1H nuclear magnetic resonance (NMR) spectra of compound **5a** as a chain-opened model and $BAPDiT^{ox}$ as a chain-closed model in the presence or absence of Ca^{2+} at pH 7.5 and 25 °C. Reaction conditions: for bottom panels, $CaCl_2$ (97 μmol) was added to solution of compound **5a** (9.7 μmol) in 100 mM Tris-HCl buffer solution at pH 7.5 (400 μL); for top panels, $CaCl_2$ (90 μmol) was added to solution of $BAPDiT^{ox}$ (9.0 μmol) in 100 mM Tris-HCl buffer solution at pH 7.5 (400 μL). ^1H NMR (500 MHz) spectra were recorded at 25 °C using a double sample tube, which comprised of an inner and outer tube including D_2O and the sample solution, respectively.

cells on or off. After K^+ and Na^+, Ca^{2+} is among the most abundant metal ions in mammals and is closely related to various biological redox reactions. In the ER, which stores high concentrations of Ca^{2+} (approximately 1 mM) (Fig. 1b, green), Ca^{2+}-binding chaperones such as calnexin and calreticulin control the quality of nascent proteins by cooperating with S–S-related oxidoreductases (i.e., PDI family proteins)[44–47]. Abnormal fluctuations in Ca^{2+} concentrations in the ER cleave the cross-network between ER-resident enzymes and contribute to the generation of misfolded proteins, eventually causing various human diseases, including neurodegenerative disorders (Fig. 1b, green)[48–50]. In addition, excessive release of Ca^{2+} from the ER into the cytosol increases the mitochondrial Ca^{2+} concentration via Ca^{2+}-transportation systems, such as the mitochondrial Ca^{2+} uniporter, eventually leading to ROS production and subsequent oxidative modification and misfolding of proteins (Fig. 1b, yellow)[51,52].

In this study, we synthesized allosteric S–S- and Se–Se-based redox reagents and catalysts that modulate their activity in response to a change in the Ca^{2+} concentration (Fig. 2b) (see the next section for the design concept). Subsequently, we demonstrated in vitro up- and down-regulation of kinetics for three representative bio-related redox reactions: (I) oxidative protein folding, (II) reductive antioxidation, and (III) reductive protein degradation, using synthetic allosteric catalysts (Fig. 1c). Finally, we conducted in-cell investigations to demonstrate that allosteric catalysts can contribute to redox homeostasis and protect against redox imbalance induced by fluctuations in Ca^{2+} concentrations in living cells.

Results

Synthesis of allosteric catalysts

The ethylene glycol derivative, 1,2-bis(*o*-aminophenoxy)ethane-*N*,*N*,*N*′,*N*′-tetraacetic acid (BAPTA, Fig. 2a, right), rigidly forms a symmetric octa-coordination complex with Ca^{2+} [53]. In this study, we synthesized $BAPDiT^{ox}$ and $BAPDiS^{ox}$, which are the DTT^{ox} and DST^{ox} analogs, respectively, with the BAPTA moiety as the Ca^{2+}-capturing site (Fig. 2b). The dihedral angle (τ) in the ethylene glycol moiety of BAPTA is firmly fixed by coordinating Ca^{2+} to its ligand (Fig. 2a, right)[54]. Incorporation of Ca^{2+} into the ligands of $BAPDiT^{ox}$ and $BAPDiS^{ox}$ is expected to cause substantial strain in the cyclic structures, resulting in thermodynamically destabilized S–S and Se–Se bonds, which are readily converted to the corresponding reactive reduced states in the presence of reductants (Fig. 2b).

$BAPDiT^{ox}$ and its reduced form ($BAPDiT^{red}$) were synthesized in total yields of 62% and 61%, respectively, in seven steps (Fig. 3a). A similar protocol was adopted to obtain $BAPDiS^{ox}$, which resulted in 27% overall yield over seven steps. However, the reduced form of $BAPDiS^{ox}$ ($BAPDiS^{red}$) could not be isolated because of its instability in air. All synthesized compounds were identified via spectroscopic analyses using nuclear magnetic resonance (NMR) and mass spectrometry (see Supplementary Information). To monitor the Ca^{2+}-coordinating behavior of the compounds, $BAPDiT^{ox}$ was mixed with Ca^{2+} in buffer solution at pH 7.5, and the resulting solution was analyzed using ^1H NMR (Fig. 3b). The NMR spectra showed that addition of Ca^{2+} changed the signals corresponding to the protons of the two aryl groups (Fig. 3b, top panels) in terms of both the chemical shift and coupling state. This result indicates that the structure and electronic state of the ligand were dramatically changed by coordination of Ca^{2+}. Similar spectral changes were observed for compound **5a**, an inactive model compound of $BAPDiT^{red}$ and $BAPDiS^{red}$ (Fig. 3b, bottom panels). Furthermore, ^{13}C NMR spectroscopic analysis of $BAPDiT^{ox}$ indicated that incorporation of Ca^{2+} into the ligand caused a structural change in the cyclic skeleton (Supplementary Fig. 1), strongly supporting that Ca^{2+} can function as an allosteric effector.

Table 1 | Physicochemical parameters of BAPDiT and BAPDiS.[a]

Compound ± metal ions		$E^{o\prime}$ (mV) [b]	pK_a^1 [c], pK_a^2 [d] ($pK_a^{average}$) [e]
BAPDiT	− Ca^{2+}	−378 ± 2	6.2 ± 0.1, 10.1 ± 0.1 (8.2)
	+ Ca^{2+}	−296 ± 2	6.9 ± 0.2, 9.3 ± 0.1 (8.1)
	+ Mg^{2+}	−386 ± 1	ND [f]
BAPDiS	− Ca^{2+}	−383 ± 1	ND [f]
	+ Ca^{2+}	−351 ± 2	ND [f]
DTT	− Ca^{2+}	−327	9.2, 10.1 (9.7) [g]
DST	− Ca^{2+}	−396 ± 7 [h]	ND [f]

[a]All data are shown as the mean ± standard error mean (SEM) ($n = 3$). [b]Reduction potential calculated using the Nernst equation with a DTT^{red} reduction potential of −327 mV[68]. Experiments were performed as previously described[23]. [c]Acid dissociation constant of the first thiol. [d]Acid dissociation constant of second thiol. [e]Average pK_a^1 and pK_a^2. [f]Not determined. [g]Data from ref.[69]. [h] Data from ref. 23.

Physicochemical properties of the allosteric catalysts

To quantify the allosteric effects of the synthesized compounds, their physicochemical properties in the presence and absence of Ca^{2+} were investigated. First, to evaluate the effect of Ca^{2+} on thermodynamic stability of the S–S and Se–Se bonds, their reduction potentials were measured using the redox equilibrium reaction between the compounds and DTT^{red} (Supplementary Fig. 2). In both BAPDiT and BAPDiS measurements, addition of Ca^{2+} to the sample solution significantly increased the reduction potential (Table 1). This result indicated that Ca^{2+} coordination induced ring-distortion in the oxidized forms and limited rotation of the dihedral angle (τ) in the reduced forms (Fig. 2b), thereby decreasing the relative thermodynamic stability of the S–S and Se–Se bonds. Thus, the redox capabilities of BAPDiT and BAPDiS may be up- and downregulated in situ by changing the concentration of Ca^{2+} as an allosteric effector. Furthermore, the dependency of the reduction potential on the Ca^{2+} concentration was investigated using $BAPDiS^{ox}$. The estimated reduction potential of $BAPDiS^{ox}$ was plotted against the Ca^{2+} concentration (Supplementary Fig. 3). The results indicated that for concentrations up to the 1/100 equivalent of $CaCl_2$ with respect to $BAPDiS^{ox}$, the reduction potential did not significantly increase, and that 1 to 10 equivalents of Ca^{2+} were required to sufficiently destabilize the Se–Se bond. In contrast, Mg^{2+}, a homologous divalent ion of Ca^{2+} that is abundant in living cells, did not increase the reduction potential of the compounds, suggesting that the compounds can selectively chelate Ca^{2+}. Supplementary Fig. 12 further shows the ion selectivity of the compounds. In addition, the average pK_a values of the two SH groups in $BAPDiT^{red}$ were almost identical in the presence and absence of Ca^{2+}, indicating that Ca^{2+} did not affect the acidities (nucleophilicities) of the chalcogenol groups (Table 1 and Supplementary Fig. 4).

Kinetics of biological redox reactions controlled by the allosteric catalysts

We further attempted to control the kinetics of the biological redox reactions in buffer solution by utilizing the redox tunability of BAPDiT and BAPDiS. First, the oxidative folding (Reaction I in Fig. 1c) of the reduced form of hen egg white lysozyme (HEL), which has four S–S bonds (i.e., C6–C127, C30–C115, C64–C80, and C76–C94) in the native state, was performed using the synthetic compounds as catalysts in the absence or presence of Ca^{2+}. Oxidative folding involves two chemical processes, namely S–S formation and subsequent S–S isomerization (Fig. 4a). During S–S formation, oxidation occurs in protein molecules to form non-native (misbridged) S–S bonds. In contrast, during S–S isomerization, rearrangement occurs to form the correct S–S bonding pattern found in the native state. The cyclic S–S and Se–Se moieties in the compounds promote oxidative folding in a manner similar to the catalytic mechanism of PDI. Briefly, S–S and Se–Se introduce S–S linkages into a substrate protein via an intermolecular bond exchange reaction (Fig. 4a; arrow highlighted in orange), whereas the SH (S^-) and SeH (Se^-) groups in $BAPDiT^{red}$ and $BAPDiS^{red}$, respectively, temporarily cleave misbridged S–S bonds to exchange the S–S positions via a mixed S–S or S–Se intermediate (Fig. 4a; arrows highlighted in green). Here, reduced HEL was incubated with $BAPDiS^{ox}$ under aerobic conditions. During oxidative folding, populations of bioactive species, including native HEL, gradually increase. Thus, the progression of oxidative folding can be estimated indirectly by estimating the relative enzymatic activity in a sample solution. The recovery of HEL enzymatic activity was estimated at specific time points, as described previously (Fig. 4b)[25]. Although the recovery of enzymatic activity was negligible in the absence of Ca^{2+}, the coexistence of Ca^{2+} dramatically accelerated the catalytic oxidative folding, yielding 45% of the active HEL after 5 h. Furthermore, Ca^{2+} concentration-dependency on foldase-like function of $BAPDiS^{ox}$ was also evaluated. When the oxidative folding of HEL was performed in the presence of various concentrations of Ca^{2+}, the foldase-like activity of BAPDiS was gradually enhanced with increasing Ca^{2+} concentration (Supplementary Fig 5). In contrast, DST^{ox}, which has no Ca^{2+} ligand, did not mediate HEL folding in neither the presence nor absence of Ca^{2+}. These observations indicate that incorporating Ca^{2+} into the compound ligand causes upregulation of cyclic Se–Se catalytic activity for oxidative folding. Slow oxidative folding typically reduces the yield of the native state because of competitive aggregation of structurally immature folding intermediates. Interestingly, when $BAPDiS^{ox}$ was used as a catalyst in the presence of Ca^{2+}, up to 64% the enzymatic activity was recovered after 24 h, whereas under other conditions, the recovery was only 30–50%. Improved folding kinetics may have shortened the lifetime of structurally immature folding intermediates, suppressing undesired protein aggregation and resulting in higher final folding yields.

High-performance liquid chromatography (HPLC) analysis of the folding intermediates generated during the reaction was performed to further understand the oxidative folding of HEL (Fig. 4c). The HPLC chromatograms showed that the presence of Ca^{2+} in the sample solution substantially accelerated both the oxidation of reduced HEL and subsequent generation of native HEL. This result suggests that $BAPDiS^{ox}$, whose oxidizability was enhanced by incorporation of Ca^{2+}, promoted S–S formation in the substrate protein and $BAPDiS^{red}$, which was generated in the solution, catalyzed S–S isomerization to form the correct S–S-bonding pattern (Fig. 4a). Similar enhancement of oxidative folding in the presence of Ca^{2+} was observed in experiments using BAPDiT (Supplementary Fig. 6a). Notably, oxidative folding promoted by BAPDiT and BAPDiS with Ca^{2+} was decelerated by addition of EDTA, a non-specific chelator of divalent metal ions, and re-accelerated upon further Ca^{2+} addition (Supplementary Fig. 6b, c). Thus, the kinetics of oxidative folding mediated by synthetic compounds may be precisely controlled using Ca^{2+} as a trigger switch.

To further explore the functions of the synthesized compounds, we evaluated their reductase-like activity against ROS (Reaction II in Fig. 1c) and protein S–S bonds (Reaction III in Fig. 1c). In these assays (Fig. 4d), cyclic S–S or Se–Se is converted by coexisting GSH into the corresponding dithiol and diselenol states, which then reduce H_2O_2 or insulin S–S bonds as substrates through GPx- and PDI-like functions, respectively[55,56]. Generated oxidized GSH (GSSG) is quickly reduced back to GSH with NADPH by glutathione reductase. Thus, the reductase-like activity of the compounds was evaluated by monitoring changes in absorbance at 340 nm due to consumption of NADPH.

In the reduction of H_2O_2 (Supplementary Fig. 7a, b), $BAPDiT^{ox}$ did not promote the reaction in the presence and absence of Ca^{2+}. In contrast, the initial velocity increased by 1.7-fold in the presence of $BAPDiS^{ox}$, a selenium analog, compared with that observed in the control sample in the absence of the catalyst (Fig. 4e). These trends were not consistent with the order of the reduction potentials of the compounds. This result suggests that not only the thermodynamics of the S–S and Se–Se bonds, but also the kinetics for activation to the chalcogenol forms is an important determinant of the catalytic reaction velocity[28]. More importantly, addition of Ca^{2+} further enhanced the initial reaction velocity by 1.1-fold compared with that observed in the absence of Ca^{2+} (blue bars in Fig. 4e). Furthermore, the

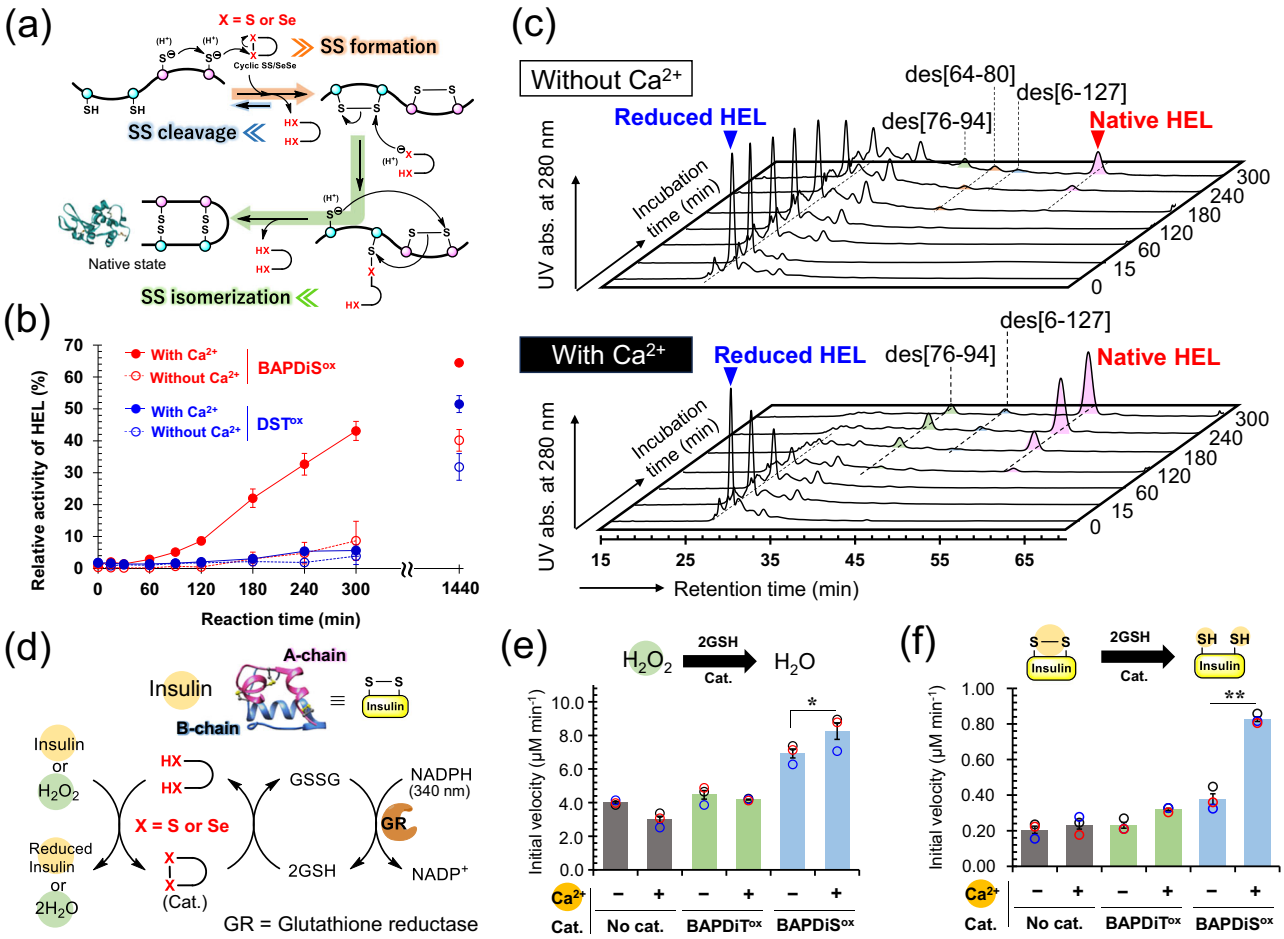

Fig. 4 | PDI- and GPx-like activity of synthetic compounds regulated by Ca^{2+} as an allosteric effector. a General oxidative folding mechanisms. **b** Time course of recovered enzymatic activity of HEL during oxidative folding of reduced HEL using $BAPDiS^{ox}$ (red) or DST^{ox} (blue) as a catalyst in the presence (solid line) or absence (dashed line) of Ca^{2+}. Reaction conditions: $[reduced\ HEL]_0 = 10\ \mu M$, $[BAPDiS^{ox}]_0$ or $[DST^{ox}]_0 = 20\ \mu M$ in 100 mM Tris-HCl buffer solution containing no or 1 mM $CaCl_2$ at 37 °C and pH 7.5 in the presence of 2 M urea under aerobic conditions. Data are shown as the means ± SEM ($n = 3$). **c** High-performance liquid chromatography (HPLC) chromatograms obtained from oxidative folding of reduced HEL using $BAPDiS^{ox}$ in the absence (top) or presence (bottom) of Ca^{2+}. The reaction conditions were the same as those in (**b**). Des intermediates, des[6-127], des[64–80], and des[76–94], represents key precursors of native HEL having three native S–S bonds but lacking one S–S linkage denoted in the brackets[65–67]. **d** Reductase-like function of compounds for reduction of H_2O_2 and protein S–S bonds coupled with NADPH oxidation. **e** Comparison of initial velocity for catalytic reduction of H_2O_2. Reaction conditions: $[H_2O_2]_0 = 0.25$ mM, $[GSH]_0 = 4.0$ mM, $[NADPH]_0 = 0.3$ mM, [GR] = 4 unit mL^{-1}, and [Cat.] = 0.1 mM at 25 °C and pH 7.2 in 100 mM Tris-HCl buffer solution containing 0.9 mM EDTA with or without 1.83 mM $CaCl_2$. **f** Comparison of initial velocity for catalytic reduction of S–S bond in insulin. Reaction conditions: $[insulin]_0 = 60\ \mu M$, $[GSH]_0 = 3.7$ mM, $[NADPH]_0 = 0.12$ mM, [GR] = 4 unit mL^{-1}, and [Cat.] = 30 μM at 25 °C and pH 7.2 in 100 mM Tris-HCl buffer solution containing 0.9 mM EDTA with or without 1.83 mM $CaCl_2$.

catalytic activity of $BAPDiS^{ox}$ was enhanced with increasing Ca^{2+} concentrations (Supplementary Fig. 7c). This result suggests that Ca^{2+} functioned as an allosteric effector and assisted in ring-opening of the cyclic Se–Se bond with GSH, resulting in enhanced catalytic function. Nevertheless, Ca^{2+} only slightly increased reactivity, likely because another catalytic pathway involving direct reduction of H_2O_2 by Se–Se (i.e., -Se–Se - + H_2O_2 → -Se(=O)–Se- + H_2O [Supplementary Fig. 8]) was dominant in this reaction, as reported previously[29]. A similar trend was observed in catalytic reduction of H_2O_2 using DTT^{red} as the thiol co-substrate instead of GSH (Supplementary Fig. 9).

To further evaluate the function of allosteric compounds as reductase-like catalysts, catalytic S–S reduction was monitored using insulin as a model substrate (Supplementary Fig. 10a, b). Similar trends to those observed in the catalytic reduction of H_2O_2 were observed, but the reactivity enhancement by Ca^{2+} was more dramatic. Namely, addition of Ca^{2+} enhanced the initial reaction velocity by more than two-fold (blue bars in Fig. 4f). In addition, the catalytic activity of $BAPDiS^{ox}$ was enhanced with increasing Ca^{2+} concentrations (Supplementary Fig. 10c). This trend is consistent with that observed for Ca^{2+} concentration-dependency on the reduction potential of $BAPDiS^{ox}$ (Supplementary Fig. 3). This result indicates that Ca^{2+} can also upregulate the S–S-reductase-like activity of $BAPDiS^{ox}$.

Ca^{2+}-association of the allosteric catalysts in living cells

Taking advantage of the redox tunability of $BAPDiS^{ox}$ and $BAPDiT^{ox}$, these compounds may be applied as biocompatible allosteric catalysts that exhibit oxidoreductase-like activity only under specific physiological conditions in cells (Fig. 1b). To allow $BAPDiT^{ox}$ and $BAPDiS^{ox}$ to permeate the cell membrane, these compounds were treated with bromomethyl acetate, thereby protecting the four carboxylic groups with acetoxymethyl (AM) esters (Fig. 5a). The AM-protected compounds, $BAPDiT^{ox}$-AM and $BAPDiS^{ox}$-AM, are hydrolyzed by cytosolic esterases after penetrating cells (Supplementary Fig. 11), and then the allosteric effect should be induced by chelating intracellular Ca^{2+}. To confirm the Ca^{2+}-chelating behavior of $BAPDiT^{ox}$ and $BAPDiS^{ox}$ in living cells, a redox-inactive model compound **9** with a rhodamine-type chromophore group was also synthesized (see Supplementary Information for synthesis details). Compound **9** emitted strong orange-yellow fluorescence at 580 nm under excitation at 558 nm because of inhibition of

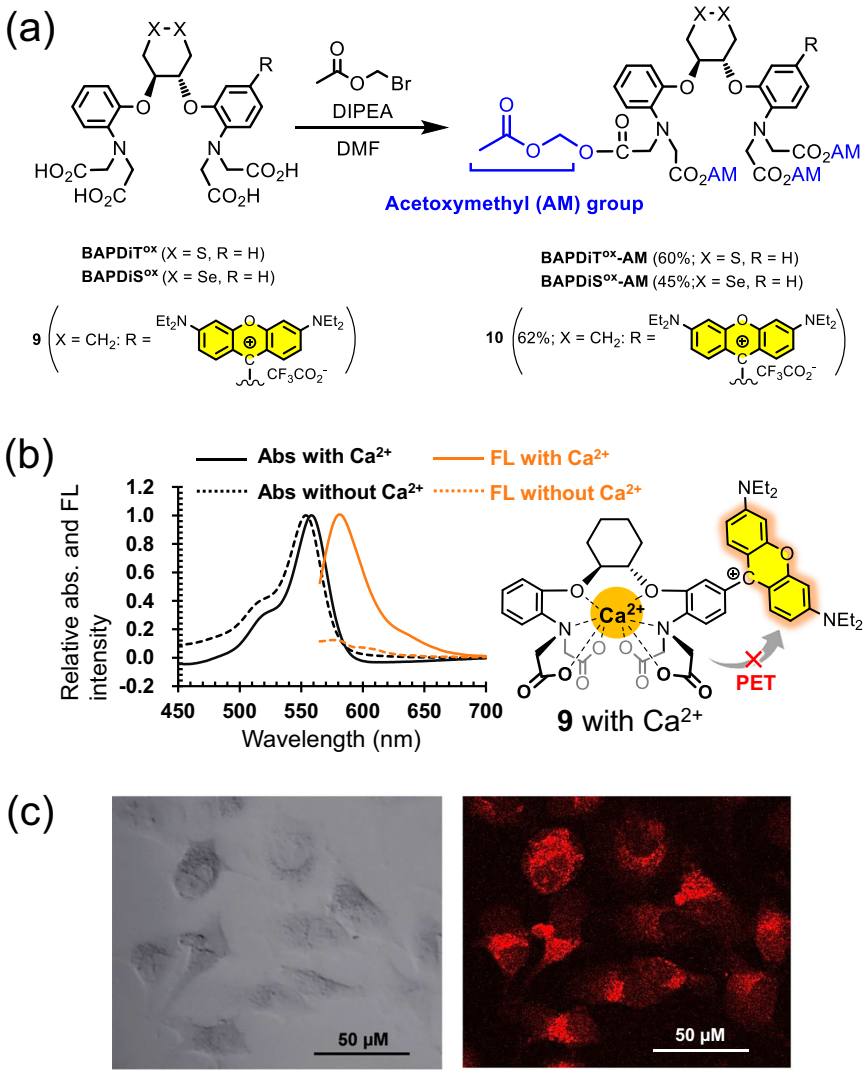

Fig. 5 | Preparation of cell membrane-permeable compounds. a Modification of BAPDiT^{ox}, BAPDiS^{ox}, and fluorescent compound **9** to acetoxymethyl (AM)-protected compounds. **b** Absorption spectra of compound **9** (5 μM) in the absence (black dashed line) and presence (black solid line) of Ca^{2+} (30 μM) and fluorescence emission spectra of compound **9** (5 μM) in the absence (orange dashed line) and presence (orange solid line) of Ca^{2+} (30 μM). The spectra were recorded using a quartz cell (path length = 10 mm) under excitation at 550 nm. The samples were prepared in 50 mM HEPES buffer solution (pH 7.5) with or without Ca^{2+}. **c** Bright-field (left) and confocal fluorescence (right) microscopy images of HeLa cells incubated with compound **10** (2.0 μM) (λ_{ex} = 561 nm; λ_{em} = 570–620 nm).

photoinduced electron transfer (PET[57,58]) by incorporating Ca^{2+} into the ligand (Fig. 5b). Other chemical properties of this compound, such as the dissociation constant (K_d) and metal ion selectivity, are summarized in the Supplementary Information (Supplementary Figs. 12 and 13 and Supplementary Table 1). HeLa cells were cultured in Hank's balanced salt solution (HBSS) containing **10**, which is AM-protected **9** (Fig. 5a), in the presence of Pluronic® F-127 for 30 min. After replacing the medium with HBSS containing Ca^{2+} and culturing the cells for 30 min, fluorescence imaging was performed using a confocal fluorescence microscope. Fluorescence staining of HeLa cells clearly indicated that compound **9**, which was generated by hydrolysis of **10** in the cells, captured intracellular Ca^{2+} (Fig. 5c). In addition, when BAPTA-AM was subsequently added to the medium, the fluorescence intensity significantly decreased (Supplementary Fig 14), suggesting that BAPTA withdrew Ca^{2+} from compound **9** in cells and/or reduced the intracellular Ca^{2+} concentration. This model study supports that the fluorescence depends on intracellular Ca^{2+} and indicates that BAPDiT^{ox} and BAPDiS^{ox} could also capture intracellular Ca^{2+} via their BAPTA-type ligand.

Crosstalk of allosteric catalysts with cellular redox systems

We examined the potential contributions of BAPDiT^{ox}-AM and BAPDiS^{ox}-AM to cellular homeostasis maintenance involving biological redox reactions. DST^{ox} with no Ca^{2+} ligand and AM-protected BAPTA (BAPTA-AM) with no redox site were used as reference samples. When HeLa cells were cultured with different concentrations of the synthetic compounds, no cytotoxicity was observed at concentrations up to 10 μM, suggesting that the compound did not adversely affect the steady-state of living cells (Fig. 6a and Supplementary Fig. 15).

Subsequently, to evaluate the function of BAPDiT^{ox} and BAPDiS^{ox} as alternative molecules for PDI in the ER, HeLa cells were incubated for 24 h in medium containing 2-[[4-(cyclopropanecarbonyl)piperazin-1-yl] methyl]-1,2-benzothiazol-3-one (LOC14[59]), a potent inhibitor of PDI (see Supplementary Fig. 16a for cytotoxicity examination of LOC14), along with compound (10 or 50 μM). The 3-(4,5-dimethyl-2-thiazolyl)-2,5-diphenyltetrazolium bromide (MTT) assay showed that cell viability was not improved following BAPDiT^{ox}-AM and BAPDiS^{ox}-AM treatments (Supplementary Fig. 17), presumably because anionic BAPDiT^{ox} and BAPDiS^{ox}, which are generated by cytosolic hydrolysis of AM-protected compounds, cannot penetrate the ER membrane. Alternatively, these compounds may not be active enough in the intracellular environment to maintain the quality control of proteins in the ER but can exhibit good PDI-like activity under optimized conditions in a test tube (Fig. 4b, c and Supplementary Fig. 6). Interestingly, DST^{ox}, an electrically neutral compound, significantly improved cell viability (Supplementary Fig. 17). However, further analyses are necessary to identify the molecular mechanisms by which DST^{ox} suppresses cell death.

Next, to validate the reductase-like activity of the synthetic compounds in living cells, oxidative stress was induced by inhibiting sarco/endoplasmic reticulum Ca^{2+}-ATPase (SERCA). SERCA is a typical P-type ATPase present in the ER membrane that pumps Ca^{2+} from the cytosol, where Ca^{2+} is

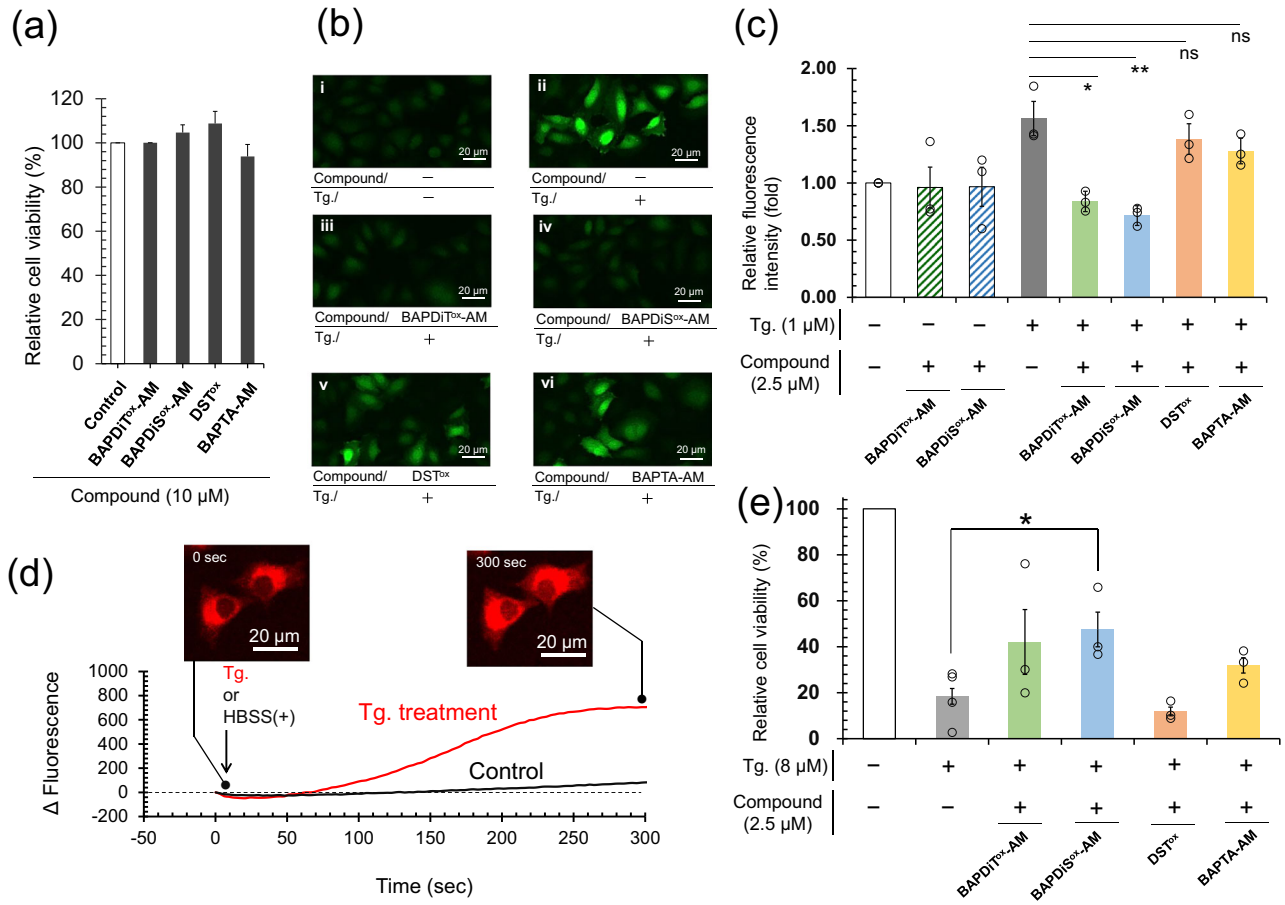

Fig. 6 | Cell experiments using synthetic compounds. a Cytotoxicity of compounds at 10 μM determined using MTT assay with HeLa cells (1×10^4 cells/well) cultured at 37 °C and 5% CO_2 for 15 h. Each independent experiment was performed in triplicate. All data of bars are shown as the mean ± SEM ($n = 3$). **b** Confocal laser scanning microscopic images of HeLa cells. HeLa cells (1×10^4 cells/well) were treated with Tg (1 μM or none) for 1 h after pretreatment with the synthetic compounds (2.5 μM or none) for 1 h and then stained with highly sensitive DCFH-DA dye® by according to the manufacturer's protocol. **c** Quantitative estimation of ROS levels in HeLa cells using a fluorescence microplate reader (excitation: 500 nm, emission: 530 nm). Stained HeLa cells were obtained using the same protocol as those in (**b**). Each independent experiment was performed in triplicate. White and gray bars are positive and negative control groups, respectively. All data are shown as the mean ± SEM (n = 3). *P* value was obtained using *t* test. **d** Change in fluorescent intensity observed through time-laps analysis using a confocal laser scanning microscope. HeLa cells (3×10^5 cells) seeded in a dish (φ 35 mm) that had been preincubated with compound **10** (2 μM) at 37 °C and 5% CO_2 for 1 h were stimulated with or without Tg (1 μM). **e** Cell viability of HeLa cells (1×10^4 cells/well) incubated with Tg (0 or 8 μM) for 20 h after pretreatment with the synthetic compounds (0 or 2.5 μM) at 37 °C and 5% CO_2 for 1 h. Cell experiments were performed at least three times. Each independent experiment was performed in triplicate. White and gray bars are positive and negative control groups, respectively. All data are shown as the mean ± SEM. *P* value was obtained using student's *t* test.

present at low concentrations (< 100 nmol), to the ER against the Ca^{2+} concentration gap[60,61]. SERCA dysfunction leads to an abnormal increase in cytosolic and mitochondrial Ca^{2+} concentrations through several pathways involving the mitochondrial Ca^{2+} uniporter and mitochondria-associated ER membranes and subsequent overproduction of ROS via mitochondrial dysfunction (Fig. 1b)[52]. This process is closely associated with several chronic diseases, such as cancer, diabetes, neurodegenerative diseases, and muscular dystrophy[62]. Synthetic compounds that exhibit remarkable foldase- and reductase-like activity only in the presence of Ca^{2+} as a trigger switch have ideal chemical properties to resist SERCA-related diseases, both in terms of regulation of the cytosolic Ca^{2+} concentration and redox control.

HeLa cells preincubated in medium with or without the compounds (2.5 μM) were treated with thapsigargin[63] (Tg; 1 μM), a potent inhibitor of SERCA (see Supplementary Fig. 16b for cytotoxicity examination of Tg). Cellular ROS levels were measured using DCFH-DA dye® (Dojindo, Kumamoto, Japan). Treatment of HeLa cells with Tg substantially increased ROS levels, as evidenced by an increase in fluorescence intensity (Fig. 6b-ii). In contrast, pretreatment of cells with BAPDiT^{ox}-AM and BAPDiS^{ox}-AM suppressed the increase in fluorescence intensity (Fig. 6b-iii and 6b-iv). Notably, DST^{ox} and BAPTA-AM, which lack the ligand for Ca^{2+} and redox site, respectively, were less capable than BAPDiT^{ox}-AM or BAPDiS^{ox}-AM in reducing ROS levels (Fig. 6b-v and -vi).

To quantify total ROS levels, the fluorescence intensity of the cultured HeLa cells was measured using a fluorescence microplate reader. The results confirmed that BAPDiT^{ox}-AM and BAPDiS^{ox}-AM effectively suppressed the Tg-induced increase in ROS levels in HeLa cells (green and blue bars in Fig. 6c). Notably, pretreatment with BAPDiT^{ox}-AM and BAPDiS^{ox}-AM did not change the total ROS level in cells at steady-state compared to that in the control group (white bar vs striped bars in Fig. 6c), indicating that the compounds did not affect the steady redox status in living cells. Although DST^{ox} and BAPTA-AM slightly decreased ROS levels, their effects were modest (orange and yellow bars in Fig. 6c). The sum of ROS levels reduced by DST^{ox} and BAPTA-AM was significantly smaller than that observed for BAPDiT^{ox}-AM and BAPDiS^{ox}-AM. This result indicated that the remarkable ROS-reducing capability of BAPDiT^{ox}-AM and BAPDiS^{ox}-AM was conferred by the synergetic effect of fusion of the Ca^{2+} ligand and redox active site. Compound **10**, a redox-inactive model compound for BAPDiT^{ox}-AM and BAPDiS^{ox}-AM, increased its own fluorescence intensity with increasing cytosolic Ca^{2+} concentration, which was induced by SERCA inhibition with Tg (Fig. 6d). Collectively, these observations provide

circumstantial evidence that the cyclic S–S or Se–Se moiety, which is allosterically activated by chelating Ca^{2+} into the ligand, regulates the cytosolic redox balance, possibly through its reductase-like activity, as shown in Fig. 4e, f. Moreover, BAPDiT^{ox}-AM and BAPDiS^{ox}-AM were mostly inactive against oxidative stress in HeLa cells directly induced by H_2O_2 treatment, implying that a high level of Ca^{2+} in the cytosol is essential for the compound's reductase-like activities (Supplementary Fig. 18).

However, in assessment of hydroperoxidase-like activity, Ca^{2+} did not substantially increase the activity of BAPDiS^{ox} (Fig. 4e). This result implies that the compounds mainly act as S–S-reductase-like catalysts, indirectly enhancing the intracellular antioxidative potential by activating cytosolic antioxidant enzymes, such as glutaredoxin and thioredoxin, with Cys-Xaa-Xaa-Cys (Xaa = an amino acid) motifs in their active centers, rather than directly scavenging ROS through hydroperoxide-like functions. In contrast to our initial assumption, BAPDiT^{ox}, which was inactive in the hydroperoxide- and S–S-reductase-like activity assays (Fig. 4e, f), was also effective in regulating the redox balance in HeLa cells. This result suggests that the S–S and Se–Se bond thermodynamics of the compounds (Table 1, Supplementary Fig. 2c) is responsible for regulating the redox balance in cells, whereas the kinetics for active chalcogenol state generation is a major determinant of the catalytic reaction rate (Fig. 4e, f). Importantly, when HeLa cells pre-incubated with BAPDiS^{ox}-AM for 1 h were treated with Tg for 22 h, cell viability was significantly improved compared with that in the control group (Fig. 6e). Our observations suggest that the allosteric redox compounds proposed in the present study are candidate therapeutic agents for a variety of diseases associated with redox imbalance induced by SERCA pump dysfunction. However, further studies are warranted to evaluate the molecular mechanisms in greater detail.

Discussion

Through molecular design of cyclic S–S/Se–Se compounds fused with BAPTA-type ligands, we developed artificial allosteric redox catalysts activated by Ca^{2+} as a trigger switch. Selective incorporation of Ca^{2+} into the ligand led to a strain of cyclic dichalcogenide, which was readily converted into the corresponding highly reactive chain-opened dichalcogenols possessing reductase and foldase activities. By adjusting the concentration of Ca^{2+} in the solution, the kinetics of the three model reactions (Fig. 1c), oxidative protein folding, reductive antioxidation, and reductive protein degradation, were precisely controlled. At a low Ca^{2+} concentration, the compound existed as an almost stable dichalcogenide (OFF state, Fig. 1b) and therefore did not affect homeostasis in normal cells. In contrast, in specific situations where cytosolic Ca^{2+} concentrations were elevated, the compounds were converted into the activated state (ON state, Fig. 1b) because of their allosteric effect and resisted the redox imbalance induced by ROS generation. However, mechanistic evidence showing that the compounds can directly exert reductase- and foldase-like activity in living cells has not been obtained, although we provide sufficient data on the functions of the compounds from several in vitro experiments. Additionally, in vivo studies are needed to accumulate more detailed biological insights into organelles in which the compounds can localize and function prior to further validating the utility of the compounds.

In conventional catalytic chemistry, catalytic reactivity and cytotoxicity have a trade-off relationship, rendering their biological use extremely difficult[41,64]. The successful development of cell-driven catalysts that can up- or downregulate their bioactivity in response to a cellular environment will provide a foundation for the development of small molecular machinery that can promote a specific reaction in the desired location at the required time. Changing the type of allosteric effector and its selectivity by modifying the structure of the metal ion ligand is also expected to be possible. Furthermore, by incorporating the concept of drug delivery systems into allosteric catalysts, the molecules can potentially be used as prodrugs targeting specific tissues and organelles. We are currently seeking to develop a new class of allosteric catalysts that can be practically applied as prodrugs for the treatment of redox-related disorders, such as muscular dystrophy and neurodegenerative diseases.

Methods

All experimental details, including synthesis methods, reduction potential measurements, pK_a measurements, oxidative folding assays, oxidoreductase-like activity assays, cell cultures, cellular imaging, cytotoxicity assays, and quantification of total ROS in living cells, are provided in *Experimental* (section 1) in the Supplementary Information.

Reporting summary

Further information on research design is available in the Nature Portfolio Reporting Summary linked to this article.

Data availability

Data supporting the findings of this study are provided in the main text. All spectral data of synthetic compounds (section 2) and further evidence for this research (section 3) are provided in the Supplementary Information. All data are available from the corresponding author upon reasonable request.

Received: 3 October 2024; Accepted: 24 February 2025;
Published online: 11 March 2025

References

1. Roberts, C. K. & Sindhu, K. K. Oxidative stress and metabolic syndrome. *Life Sci.* **84**, 705–712 (2009).
2. Rani, V., Deep, G., Singh, R. K., Palle, K. & Yadav, U. C. S. Oxidative stress and metabolic disorders: pathogenesis and therapeutic strategies. *Life Sci.* **148**, 183–193 (2016).
3. Masenga, S. K., Kabwe, L. S., Chakulya, M. & Kirabo, A. Mechanisms of oxidative stress in metabolic syndrome. *Int. J. Mol. Sci.* **24**, 7898 (2023).
4. Hartl, F. U. Protein misfolding diseases. *Annu. Rev. Biochem.* **86**, 21–26 (2017).
5. Herrera, M. I. et al. Neuroprotection targeting protein misfolding on chronic cerebral hypoperfusion in the context of metabolic syndrome. *Front. Neurosci.* **12**, 1–9 (2018).
6. Lin, J.-A., Wu, C.-H., Lu, C.-C., Hsia, S.-M. & Yen, G.-C. Glycative stress from advanced glycation end products (AGEs) and dicarbonyls: An emerging biological factor in cancer onset and progression. *Mol. Nutr. Food Res.* **60**, 1850–1864 (2016).
7. Egawa, T. & Hayashi, T. Association of Glycative stress with motor and muscle function. *Front. Physiol.* **13**, 855358 (2022).
8. Robertson, K. D. & Wolffe, A. P. DNA methylation in health and disease. *Nat. Rev. Genet.* **1**, 11–19 (2000).
9. Jin, Z. & Liu, Y. DNA methylation in human diseases. *Genes. Dis.* **5**, 1–8 (2018).
10. Delaunay, S., Helm, M. & Frye, M. RNA modifications in physiology and disease: towards clinical applications. *Nat. Rev. Genet.* **25**, 104–122 (2024).
11. Kuah, E., Toh, S., Yee, J., Ma, Q. & Gao, Z. Enzyme mimics: advances and applications. *Chem. Eur. J.* **22**, 8404–8430 (2016).
12. Traut, T. Enzyme Activity: Allosteric Regulation. in *Encyclopedia of Life Sciences* (John Wiley & Sons, Ltd, 2014). https://doi.org/10.1002/9780470015902.a0000865.pub3.
13. Blanco, V., Leigh, D. A. & Marcos, V. Artificial switchable catalysts. *Chem. Soc. Rev.* **44**, 5341–5370 (2015).
14. van Dijk, L. et al. Molecular machines for catalysis. *Nat. Rev. Chem.* **2**, 1–18 (2018).
15. Pan, T., Wang, Y., Xue, X. & Zhang, C. Rational design of allosteric switchable catalysts. *Exploration* **2**, 20210095 (2022).
16. Thaggard, G. C., Haimerl, J., Fischer, R. A., Park, K. C. & Shustova, N. B. Traffic lights for catalysis: stimuli-responsive molecular and extended catalytic systems. *Angew. Chem. Int. Ed.* **62**, e202302859 (2023).
17. Butler, R. N. & Coyne, A. G. Water: nature's reaction enforcer—comparative effects for organic synthesis "in-water" and "on-water". *Chem. Rev.* **110**, 6302–6337 (2010).

18. van der Helm, M. P., Klemm, B. & Eelkema, R. Organocatalysis in aqueous media. *Nat. Rev. Chem.* **3**, 491–508 (2019).
19. Das, N. & Maity, C. Switchable aqueous catalytic systems for organic transformations. *Commun. Chem.* **5**, 1–23 (2022).
20. Ghorbani-Choghamarani, A. & Taherinia, Z. Recent advances utilized in artificial switchable catalysis. *RSC Advances* **12**, 23595–23617 (2022).
21. Cao, S. S. & Kaufman, R. J. Endoplasmic reticulum stress and oxidative stress in cell fate decision and human disease. *Antioxid. Redox Signal.* **21**, 396–413 (2014).
22. Ong, G. & Logue, S. E. Unfolding the interactions between endoplasmic reticulum stress and oxidative stress. *Antioxidants* **12**, 981 (2023).
23. Arai, K. et al. Protein folding in the presence of water-soluble cyclic diselenides with novel oxidoreductase and isomerase activities. *ChemBioChem* **19**, 207–211 (2018).
24. Okada, S. et al. Coupling effects of thiol and urea-type groups for promotion of oxidative protein folding. *Chem. Commun.* **55**, 759–762 (2019).
25. Tsukagoshi, S., Mikami, R. & Arai, K. Basic amino acid conjugates of 1,2-diselenan-4-amine with protein disulfide isomerase-like functions as a manipulator of protein quality control. *Chem. Asian J.* **15**, 2646–2652 (2020).
26. Okada, S. et al. Semi-enzymatic acceleration of oxidative protein folding by *N*-methylated heteroaromatic thiols. *Chem. Sci.* **14**, 7630–7636 (2023).
27. Kuramochi, T. et al. Boosting the enzymatic activity of CxxC motif-containing PDI family members. *Chem. Commun.* **60**, 6134–6137 (2024).
28. Arai, K. et al. Modeling thioredoxin reductase-like activity with cyclic selenenyl sulfides: participation of an NH···Se hydrogen bond through stabilization of the mixed Se−S intermediate. *Chem. Eur. J.* **25**, 12751–12760 (2019).
29. Arai, K. et al. Glutathione peroxidase-like functions of 1,2-diselenane-4,5-diol and its amphiphilic derivatives: switchable catalytic cycles depending on peroxide substrates. *Bioorg. Med. Chem.* **29**, 115866 (2021).
30. Wilkinson, B. & Gilbert, H. F. Protein disulfide isomerase. *Biochim. Biophys. Acta - Proteins and Proteomics* **1699**, 35–44 (2004).
31. Gruber, C. W., Čemažar, Heras, M., Martin, B. & Craik, J. L. D. J. Protein disulfide isomerase: the structure of oxidative folding. *Trends Biochem. Sci.* **31**, 455–464 (2006).
32. Oka, O. B. V. & Bulleid, N. J. Forming disulfides in the endoplasmic reticulum. *Biochim. Biophys. Acta - Mol. Cell. Res.* **1833**, 2425–2429 (2013).
33. Wang, L., Wang, X. & Wang, C. Protein disulfide–isomerase, a folding catalyst and a redox-regulated chaperone. *Free Radic. Biol. Med.* **83**, 305–313 (2015).
34. Okumura, M., Watanabe, S. & Inaba, K. *Oxidative Folding of Proteins: Basic Principles, Cellular Regulation and Engineering* Ch. 3(Royal Society of Chemistry, Cambridge, 2018).
35. Okumura, M., Noi, K. & Inaba, K. Visualization of structural dynamics of protein disulfide isomerase enzymes in catalysis of oxidative folding and reductive unfolding. *Curr. Opin. Struct. Biol.* **66**, 49–57 (2021).
36. Wang, L. & Wang, C. Oxidative protein folding fidelity and redoxtasis in the endoplasmic reticulum. *Trends Biochem. Sci.* **48**, 40–52 (2023).
37. Narayan, M., Welker, E., Wedemeyer, W. J. & Scheraga, H. A. Oxidative folding of proteins. *Acc. Chem. Res.* **33**, 805–812 (2000).
38. Flohe, L., Günzler, W. A. & Schock, H. H. Glutathione peroxidase: a selenoenzyme. *FEBS Lett* **32**, 132–134 (1973).
39. Brigelius-Flohé, R. & Maiorino, M. Glutathione peroxidases. *Biochim. Biophys. Acta - Gen. Subj* **1830**, 3289–3303 (2013).
40. Iwaoka, M. & Arai, K. From sulfur to selenium. a new research arena in chemical biology and biological chemistry. *Curr. Chem. Biol.* **7**, 2–24 (2013).
41. Arai, K. *Chalcogen Chemistry: Fundamentals and Applications* Ch. 25 (Royal Society of Chemistry, Cambridge, 2023).
42. Nogara, P. A., Pereira, M. E., Oliveira, C. S., Orian, L. & da Rocha, J. B. T. *Chalcogen Chemistry: Fundamentals and Applications* Ch. 21 (Royal Society of Chemistry, Cambridge, 2023).
43. Sancineto, L. & Nascimento, V. *Chalcogen Chemistry: Fundamentals and Applications* Ch. 22 (Royal Society of Chemistry, Cambridge, 2023).
44. Corbett, E. F. et al. Ca^{2+} regulation of interactions between endoplasmic reticulum chaperones. *J. of Biol. Chem.* **274**, 6203–6211 (1999).
45. Okumura, M. et al. A unique leucine-valine adhesive motif supports structure and function of protein disulfide isomerase P5 via dimerization. *Structure* **29**, 1357–1370 (2021). E6.
46. Li, Y. & Camacho, P. Ca^{2+}-dependent redox modulation of SERCA 2b by ERp57. *J. Cell. Biol.* **164**, 35–46 (2004).
47. Tanikawa, Y. et al. Ca^{2+} regulates ERp57-calnexin complex formation. *Molecules* **26**, 2853 (2021).
48. Andreu, C. I., Woehlbier, U., Torres, M. & Hetz, C. Protein disulfide isomerases in neurodegeneration: from disease mechanisms to biomedical applications. *FEBS Lett* **586**, 2826–2834 (2012).
49. Matsusaki, M. et al. The protein disulfide isomerase family: from proteostasis to pathogenesis. *Biochim. Biophys. Acta - Gen. Subj* **1864**, 129338 (2020).
50. Medinas, D. B., Rozas, P. & Hetz, C. Critical roles of protein disulfide isomerases in balancing proteostasis in the nervous system. *J. Biol. Chem.* **298**, 102087 (2022).
51. Ermak, G. & Davies, K. J. A. Calcium and oxidative stress: from cell signaling to cell death. *Mol. Immunol.* **38**, 713–721 (2002).
52. Görlach, A., Bertram, K., Hudecova, S. & Krizanova, O. Calcium and ROS: a mutual interplay. *Redox Biol* **6**, 260–271 (2015).
53. Tsien, R. Y. New calcium indicators and buffers with high selectivity against magnesium and protons: design, synthesis, and properties of prototype structures. *Biochemistry* **19**, 2396–2404 (1980).
54. Csomos, A. et al. A comprehensive study of the Ca^{2+} ion binding of fluorescently labelled BAPTA analogues. *Eur. J. Org. Chem.* **2021**, 5248–5261 (2021).
55. Gilbert, H. F. [3] Protein disulfide isomerase. *Methods Enzymol* **290**, 26–50 (1998).
56. Wilson, S. R., Zucker, P. A., Huang, R. R. C. & Spector, A. Development of synthetic compounds with glutathione peroxidase activity. *J. Am. Chem. Soc.* **111**, 5936–5939 (1989).
57. Roopa, Kumar, N., Kumar, M. & Bhalla, V. Design and applications of small molecular probes for calcium detection. *Chem. Asian J.* **14**, 4493–4505 (2019).
58. Zhou, X., Belavek, K. J. & Miller, E. W. Origins of Ca^{2+} imaging with fluorescent indicators. *Biochemistry* **60**, 3547–3554 (2021).
59. Kaplan, A. et al. Small molecule-induced oxidation of protein disulfide isomerase is neuroprotective. *Proc. Natl. Acad. Sci.* **112**, E2245–E2252 (2015).
60. Clarke, D. M., Loo, T. W., Inesi, G. & MacLennan, D. H. Location of high affinity Ca^{2+}-binding sites within the predicted transmembrahe domain of the sarco-plasmic reticulum Ca^{2+}-ATPase. *Nature* **339**, 476–478 (1989).
61. Toyoshima, C., Nakasako, M., Nomura, H. & Ogawa, H. Crystal structure of the calcium pump of sarcoplasmic reticulum at 2.6 Å resolution. *Nature* **405**, 647–655 (2000).
62. Xu, H. & Van Remmen, H. The sarcoendoplasmic reticulum calcium ATPase (SERCA) pump: a potential target for intervention in aging and skeletal muscle pathologies. *Skelet. Muscle* **11**, 25 (2021).
63. Sabała, P., Czarny, M., Woronczak, J. P. & Barańska, J. Thapsigargin: potent inhibitor of Ca^{2+} transport ATP-ases of endoplasmic and sarcoplasmic reticulum. *Acta Biochim. Pol.* **40**, 309–319 (1993).
64. Arai, K. & Mikami, R. Redox chemistry of selenols and diselenides as potential manipulators for structural maturation of peptides and proteins. *Metallomics Res.* **2**, 1–17 (2022).

65. van den Berg, B., Chung, E. W., Robinson, C. V. & Dobson, C. M. Characterisation of the dominant oxidative folding intermediate of hen lysozyme. *J. Mol. Biol.* **290**, 781–796 (1999).
66. van den Berg, B., Chung, E. W., Robinson, C. V., Mateo, P. L. & Dobson, C. M. The oxidative refolding of hen lysozyme and its catalysis by protein disulfide isomerase. *EMBO J* **18**, 4794–4803 (1999).
67. Arai, K., Shibagaki, W., Shinozaki, R. & Iwaoka, M. Reinvestigation of the oxidative folding pathways of hen egg white lysozyme: switching of the major pathways by temperature control. *Int. J. Mol. Sci.* **14**, 13194–13212 (2013).
68. Lees, W. J. & Whitesides, G. M. Equilibrium constants for thiol-disulfide interchange reactions: a coherent, corrected set. *J. Org. Chem.* **58**, 642–647 (1993).
69. Whitesides, G. M., Lilburn, J. E. & Szajewski, R. P. Rates of thiol-disulfide interchange reactions between mono- and dithiols and Ellman's reagent. *J. Org. Chem.* **42**, 332–338 (1977).

Acknowledgements

This work was supported by the Japan Society for the Promotion of Science (JSPS) [KAKENHI: grant number 23K04933 (to KA) and 24KJ2003 (to RM)], Promotion and Mutual Aid Corporation for Private Schools of Japan (PMAC) [Science Research Promotion Fund (to KA)], and Research and Study Project of Tokai University, Educational System General Research Organization (to KA and MO).

Author contributions

K.A. conceived and initiated the project. K.A. and R.M. designed and conducted experiments. Y.S. and S.K. cooperatively conducted synthesis of compounds and biological assays, respectively, with R.M. T.M., M.O., and K.A. supervised this study. K.A. and R.M. prepared the manuscript, which was edited by all authors.

Competing interests

The authors declare no competing interests.

Additional information

Supplementary information The online version contains supplementary material available at https://doi.org/10.1038/s42004-025-01466-6.

Correspondence and requests for materials should be addressed to Kenta Arai.

Peer review information *Communications Chemistry* thanks Chandan Maity and the other, anonymous, reviewer(s) for their contribution to the peer review of this work. Peer review reports are available.